Chemical Geology 640 (2023) 121735

Contents lists available at ScienceDirect

Chemical Geology

journal homepage: www.elsevier.com/locate/chemgeo

Variations of Sr–Nd–Hf–O isotopes and redox conditions across a Neoproterozoic arc magmatic belt in the western margin of the Yangtze craton

Junhua Yao [a,b], Wei-Guang Zhu [b,*], Chusi Li [b,c,*], Zhong-Jie Bai [b], Yan-Jun Wang [d], Lei-Luo Xu [b]

[a] Center of Deep-Sea Research & Key Laboratory of Marine Geology and Environment, Institute of Oceanology, Chinese Academy of Sciences, Qingdao 266071, China
[b] State Key Laboratory of Ore Deposit Geochemistry, Institute of Geochemistry, Chinese Academy of Sciences, Guiyang 550081, China
[c] Department of Geological and Atmospheric Sciences, Indiana University, Bloomington, IN 47405, USA
[d] State Key Laboratory of Nuclear Resources and Environment, East China University of Technology, Nanchang 330013, China

ARTICLE INFO

Editor: S Aulbach

Keywords:
Zircon U—Pb ages
Zircon Hf—O isotopes
Magmatic fO_2
Sr–Nd isotopes
Subduction magmatism
Western China

ABSTRACT

We use zircon trace elements and Hf—O isotopes, plus whole-rock chemical and Sr—Nd isotope compositions to investigate the controls on the chemistry of Neoproterozoic arc magmas. The samples are from the gabbrodiorite intrusion of the Gaojiacun mafic-ultramafic complex and from the Tongde diorite batholith of the Panxi Neoproterozoic magmatic belt in the western margin of the Yangtze craton, western China. Zircon U—Pb ages reveal that both intrusions are coeval, emplaced at ~820 Ma. Major element compositions of whole rocks and major silicate minerals indicate that the Tongde batholith formed from more evolved magma than the parental magma for the Gaojiacun intrusion. The mantle-normalized trace element patterns of whole rocks from both intrusions are similar, showing light REE enrichments and pronounced negative Nb—Ta anomalies. The Sr—Nd isotopic compositions of the whole rocks are also similar, plotting within or very close to the mantle array, indicating no to minor contamination with the upper crust. Zircon Hf—O isotopes indicate that the Gaojiacun magma has much higher ε_{Hf} (6.26 ± 0.52) and $\delta^{18}O$ (7.0 ± 0.3 ‰) than the Tongde magma (ε_{Hf} = 4.81 ± 0.39; $\delta^{18}O$ = 5.7 ± 0.2 ‰). The $\delta^{18}O$ values of the Gaojiacun zircons are also higher than the normal mantle ($\delta^{18}O$ = 5.3 ± 0.6 ‰). Zircon trace element compositions show that, despite their close spatial association (<10 km), the coeval intrusions have contrasting redox states, with the estimated fO_2 values of ΔFMQ+1.0 and ΔFMQ-0.7 for Tongde and Gaojiacun, respectively. The former is within the range of modern arc basalts, whereas the latter is lower than the average value of MORBs. The very low fO_2 of the Gaojiacun magma could be due to the presence of subducted oceanic sediments enriched in organic matter (OM) in the source or due to contamination with OM-rich sedimentary rocks in the upper crust. Since such crustal rocks have not been reported for the region, we prefer the former explanation. The preferred model is also supported by Sr–Nd–Hf–O isotopes. The results from this study reveal that both reduced and oxidized magma could be produced simultaneously in a subduction zone.

1. Introduction

The roles of arc magmatism in continental crustal growth (Gill, 1981) and ore formation (Tomkins et al., 2012; Richards, 2015) are well established for the Phanerozoic, but much less so for the Neoproterozoic and Archean, although ~20% of the present continental crust formed during the Neoproterozoic (Stern, 2008). This is mainly due to fewer studies of Neoproterozoic arc magmatic systems and associated ore systems than the younger counterparts to date. To fill such a research gap, we have carried out an integrated geochemical study of a Neoproterozoic arc magmatic system situated in the western margin of the Yangtze craton, western China.

Previous studies of the Neoproterozoic mafic-ultramafic intrusions mainly focused on the debate on the tectonic settings, such as mantle plume (e.g., Li et al., 2006) versus subduction-related magmatism (e.g., Zhou et al., 2002a, 2002b). An important consensus resulted from more recent studies is that from ~850 to ~820 Ma this region was a continental arc (e.g., Yao et al., 2018; Zhao et al., 2019). This allows us to focus on new important questions about this Neoproterozoic subduction zone, such as arc magmatic tempos and the controls on the chemistry of

* Corresponding authors.
E-mail addresses: zhuweiguang@vip.gyig.ac.cn (W.-G. Zhu), cli@indiana.edu (C. Li).

https://doi.org/10.1016/j.chemgeo.2023.121735
Received 6 July 2023; Received in revised form 13 September 2023; Accepted 14 September 2023
Available online 24 September 2023

arc magmas. Two coeval and spatially closely associated intrusions (namely the Gaojiacun gabbrodiorite intrusion and the Tongde batholith) of the Neoproterozoic arc magmatic belt are selected for this study. Zircon U—Pb ages, Hf—O isotopes and trace element compositions are used as core data, and whole-rock elemental and Sr—Nd isotope compositions plus major silicate mineral compositions are used as complementary data. The isotopic data are used to distinguish between crustal contamination and subduction inputs. Zircon trace element data are used to estimate the magmatic redox state for each intrusion. It is intriguing that the estimated redox state for the Gaojiacun intrusion is more reduced than the average MORB value, whereas the estimated redox state for the Tongde intrusion is like the typical arc basalt value. After carefully considering the potential causes, such as (1) variable subduction inputs, (2) different degrees of fractional crystallization, and (3) different degrees of crustal contamination, we conclude that different subduction input is the major reason. This study demonstrates that the combination of zircon trace elements and Hf—O isotopes is an effective tool to determine the controls on the chemistry of the magmatic arc.

2. Geological background

2.1. The Panxi Neoproterozoic arc magmatic belt

The Panxi Neoproterozoic (870–740 Ma) arc magmatic belt occurs along the western rim of the Yangtze craton, extending from west of Panzhihua to north of Kangding with a total length of ~600 km (Fig. 1a–b). The Yangtze craton comprises a basement consisting of Archean to Proterozoic crystalline layer and Mesoproterozoic folded, metamorphic layer, and a cover of Neoproterozoic to Cenozoic sedimentary sequences (Zhao et al., 2010; Gao et al., 2011; Yao et al., 2019). The Panxi Neoproterozoic arc magmatic belt is bounded by the Songpan-

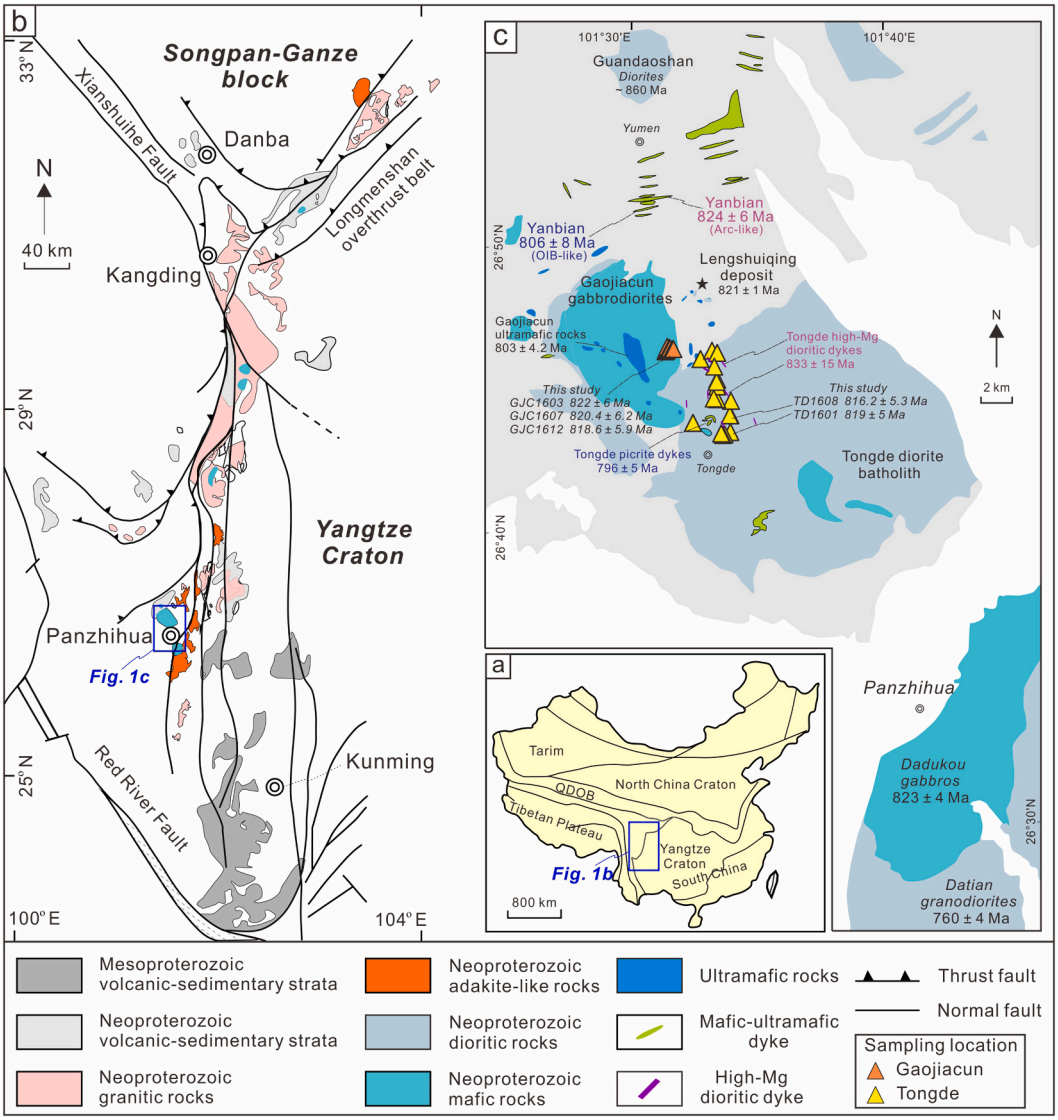

Fig. 1. (a) Schematic map showing the tectonic units of China, QDOB = Qinling-Dabie orogenic belt. (b) Simplified geologic map of the Panxi region (modified after Zhao et al., 2018), showing the distribution of igneous rocks in the Panxi Neoproterozoic arc magmatic belt. (c) Simplified geological map of the Panzhihua region (modified from Zhu et al., 2007), showing the distribution of Neoproterozoic mafic-ultramafic complexes and diorite batholiths. Zircon U—Pb ages: Guandaoshan diorites (Du et al., 2014), Gaojiacun gabbrodiorites (this study), Gaojiacun ultramafic rocks (Munteanu et al., 2010a), Lengshuiqing mafic-ultramafic rocks (Zhu et al., 2007), Tongde diorite batholith (this study), Yanbian mafic dykes (Niu et al., 2016), Tongde picrite dykes (Zhu et al., 2010), Tongde high-Mg dioritic dykes (Li and Zhao, 2018). Dadukou gabbros and Datian granodiorites (Zhao et al., 2019).

Ganzi Folded Belt (SGFB) to the north and by the Tibetan plateau to the south (Fig. 1a–b; Zhao et al., 2018). The SGFB comprises a Neoproterozoic crystalline basement and a thick sedimentary cover mainly composed of Triassic flysch sequence (e.g., Roger et al., 2010). The SGFB has a triangular shape and is bounded by the Yangtze craton to the east, the Qaidam terrane to the north, and the Qiangtang terrane to the south.

The Panxi Neoproterozoic arc magmatic belt is volumetrically dominated by large diorite and granite plutons/batholiths. Mafic-ultramafic intrusions are widespread in the region, but the sizes are much smaller than the associated diorite and granite plutons/batholiths. The granitoids generally show arc-affinity and calc-alkaline or adakitic characteristics (Zhou et al., 2002a, 2002b; Zhao et al., 2018, 2021; Huang et al., 2023; Qi et al., 2023). The mafic-ultramafic intrusions are mainly composed of gabbro, plus minor peridotites and/or diorite (Zhou et al., 2006; Zhao and Zhou, 2007; Wang et al., 2016). The mafic-ultramafic intrusions with zircon U—Pb ages older than ~820 Ma show subduction-related petrological and geochemical features (Yao et al., 2018; Zhao et al., 2018; Yao, 2019). Some of the younger mafic-ultramafic intrusions show rift-related petrological and geochemical signatures (Li et al., 2006; Zhu et al., 2008, 2010; Zhao et al., 2019; Huang et al., 2023). Originally, Li et al. (2006) and Zhu et al. (2008, 2010) suggested that they were mantle plume related. Subsequently, Yao (2019) pointed out that the plume model is inconsistent with the temporal and spatial distribution of the mafic-ultramafic intrusions. Recently, Zhao et al. (2018, 2019) and Huang et al. (2023) proposed an alternative model that they formed in a back-arc rifted or extensional environment.

2.2. The Gaojiacun mafic-ultramafic complex

The Gaojiacun and Tongde intrusive complexes are the two largest Neoproterozoic intrusive complexes in the western margin of the Yangtze craton (Fig. 1b). They intruded the early Neoproterozoic Yanbian Group that comprises flysch-type volcano-sedimentary sequences in the middle and upper parts and volcanic rocks in the lowermost part (Li et al., 2006; Du et al., 2014).

The Gaojiacun intrusive complex is elliptical on the surface, with a length of ~9 km and a width of ~7.5 km, covering an area of ~70 km^2 (Fig. 1c). It can be divided into a large outer zone and a small inner zone. The outer zone is dominated by gabbro and gabbrodiorite. The U—Pb ages of zircons from these rocks are from 806 Ma to 825 Ma (Zhu et al., 2006; Zhou et al., 2006; Munteanu et al., 2010a). The inner zone contains ultramafic intrusive rocks, such as dunite, lherzolite and troctolite. The U—Pb age of zircons from the intercalated diorite in this zone is 803 ± 4.2 Ma (Munteanu et al., 2010a). Drilling has intercepted sulfide mineralization associated with the ultramafic rocks at several depths (Zhu et al., 2006).

2.3. The Tongde intrusive complex

The Tongde intrusive complex occurs to the east of the Gaojiacun intrusive complex (Fig. 1c). The exposed area of the Tongde intrusive complex is ~300 km^2, with a diameter of ~20 km. This complex consists of a large diorite batholith, two gabbroic intrusions, numerous high-Mg diorite dykes (Li and Zhao, 2018), and several mafic-ultramafic dykes (Zhu et al., 2010). The U—Pb ages of zircons from the diorites are from 813 Ma to 845 Ma (Sun, 2009; Munteanu et al., 2010a).

3. Sample descriptions

The samples from this study were collected along a provincial road (No. 216) that runs through the Gaojiacun and Tongde complexes: 12 samples from the Gaojiacun outer zone and 25 samples from the Tongde diorite batholith (Fig. 1c). The GPS locations of the samples are given in Table S1.

The Gaojiacun samples are gabbrodiorites, composed of clinopyroxene, orthopyroxene, plagioclase, hornblende and Fe—Ti oxides, plus rare apatite (Fig. S1a–b). Hornblende crystals, 100 to 800 μm in length, occur in the interstitial spaces of pyroxenes (<300 μm in length) and plagioclase (<800 μm in length), or surrounding the rims of pyroxenes and plagioclase. Some small plagioclase grains occur as inclusions enclosed in large clinopyroxene and hornblende crystals. Some clinopyroxene grains are partially replaced by actinolite or tremolite in the fractures and grain margins.

Diorite from the Tongde batholith is composed of hornblende, plagioclase and Fe—Ti oxides, plus rare clinopyroxene and apatite (Fig. S1c–d). Large amphibole crystals (up to 1 mm in length) commonly contain small plagioclase, Fe—Ti oxide and apatite inclusions. Fine-grained Fe—Ti oxide grains are present in the center of some hornblende crystals. The only difference between diorite and quartz diorite from the Tongde batholith is the presence of minor amount of quartz in the latter.

4. Analytical methods

Zircon grains were separated from ~10 kg of each rock sample using conventional density-magnetic separation techniques, followed by handpicking under a binocular microscope. Together with zircon standard Plešovice, Penglai and Qinghu, the zircons from our samples were mounted in epoxy resin that were polished to section the crystals in half. The polished zircons were coated with gold in vacuum. Transmitted and reflected light microphotographs and cathodoluminescence (CL) images were taken to reveal the internal structures and compositional zonation of the zircon grains for target selection for in-situ analysis.

Zircon oxygen isotopic analysis was conducted on the Cameca IMS-1280 SIMS at the Ion Microprobe Laboratory of the Institute of Geology and Geophysics, Chinese Academy of Sciences (IGGCAS) in Beijing. The Cs^+ primary ion beam was accelerated at 10 kV, with an intensity of ca. 2 nA. The spot size is ~20 μm in diameter. Each spot analysis includes ~2 min pre-sputtering, ~60 s automatic beam centering, and integration of oxygen isotopes for 10 cycles × 4 s. The internal precision of $^{18}O/^{16}O$ ratios is 0.2–0.4 ‰ (2SE) from 10 cycles of measurements. Measured $^{18}O/^{16}O$ values were reported as $\delta^{18}O$ per mil (‰) values, normalized to oxygen isotopic composition of Vienna Standard Mean Ocean Water $(^{18}O/^{16}O)_{VSMOW} = 0.0020052$. The instrumental mass fractionation factor (IMF) was corrected using zircon standard Penglai with a recommended $\delta^{18}O$ value of 5.3 ± 0.1 ‰ (Li et al., 2010). Qinghu zircon was measured as an unknown to yield $\delta^{18}O$ of 5.48 ± 0.40 ‰ (2SD, $n = 33$), consistent with the recommended $\delta^{18}O$ value of 5.4 ± 0.2 ‰ (Li et al., 2013).

After oxygen isotopic analysis, the zircons were analyzed for U–Th–Pb isotopes using the same Cameca IMS-1280 SIMS at IGGCAS, following the analytical procedures of Li et al. (2009). The O_2^- primary ion beam was accelerated at 13 kV, with an intensity of ca. 8 nA. The ellipsoidal spot of the ion beam is about 20 × 30 μm in size. Analysis of zircon standard Qinghu was interspersed with the unknowns. The measured compositions are reported after correcting for common Pb using non-radiogenic ^{204}Pb. Uncertainties on individual age measurements are reported at 1σ level and the mean ages for pooled U/Pb ratios are quoted with 95% confidence interval. Data reduction was carried out using the Isoplot/Ex v. 4.15 programs (Ludwig, 2011). Qinghu zircons were analyzed to monitor the external uncertainties of SIMS U—Pb measurements, and to yield a U—Pb age of 163.4 ± 5.6 Ma that is identical within errors to the recommended value (Li et al., 2013).

Zircon Lu—Hf isotopes were conducted using a Neptune Plus multiple collector inductively coupled plasma mass spectrometer (MC-ICP-MS) with a GeoLas 2005 laser system at the State Key Laboratory of Geological Processes and Mineral Resources, China University of Geosciences (Wuhan). Detailed operating conditions and data acquisition method were similar to those described by Hu et al. (2012). Each measurement includes ~20 s background signal acquisition and ~ 50 s sample signal acquisition, and the size of a laser spot is ~44 μm in

diameter. The isobaric interference of ^{176}Lu on ^{176}Hf was corrected by monitoring the intensity of the interference-free ^{175}Lu isotope ($^{176}Lu/^{175}Lu = 0.02656$; Blichert-Toft and Albarède, 1997). The interference of ^{176}Yb on ^{176}Hf was corrected by measuring the interference-free ^{173}Yb isotope ($^{176}Yb/^{173}Yb = 0.79639$; Fisher et al., 2014). Each run of analysis for ten samples was followed by analyzing an external standard zircon 91,500 twice. A total of 32 repeating analysis of the standard zircon 91,500 from this study yielded the $^{176}Hf/^{177}Hf$ of 0.282308 ± 0.000003, which is in good agreement with the recommended $^{176}Hf/^{177}Hf$ of 0.282306 ± 0.000010 (Woodhead et al., 2004). Zircon GJ-1 and TEMORA-1 were also analyzed as the secondary quality-control standards and yielded average $^{176}Hf/^{177}Hf$ ratios of 0.281987 ± 0.000012 and 0.282684 ± 0.000018, respectively, which are within uncertainty of the recommended values from Morel et al. (2008) and Woodhead et al. (2004). Offline data reduction of signal selection, integration of selected signals and mass bias calibrations, was carried out using the ICPMSDataCal software (Liu et al., 2010).

Zircon trace element compositions were conducted by laser ablation-inductively coupled plasma-mass spectrometry (LA–ICP–MS) at the State Key Laboratory of Ore Deposit Geochemistry (SKLODG), Institute of Geochemistry, Chinese Academy of Sciences (IGCAS). An Agilent 7700× ICP–MS instrument was used to acquire ion-signal intensities. Laser conditions were 8 J/cm^2 of laser energy, 6 Hz of ablation frequency and 32 μm of spot diameter. The detailed analytical procedure was the same as that described by Liu et al. (2010) and Xu et al. (2022). Zircon 91,500 and SRM610 was used as external standards and the stoichiometric zircon SiO_2 content for internal standardization. Off-line selection and integration of background and analyte signals, and time-drift correction and quantitative calibration were performed using the ICPMSDataCal software of Liu et al. (2010).

Chemical compositions of minerals were determined by wavelength dispersive analysis using a JEOL JXA-8230 electron microprobe at the School of Resources and Environmental Engineering, Hefei University of Technology, China. The analytical conditions were 15 kV accelerating voltage, 20 nA beam current, 3–5 μm beam diameter, and 10–20 s peak counting time. The analytical precision is better than 3% for major elements (>1 wt%) and 10% for trace elements (<1 wt%). The Fe^{2+} and Fe^{3+} contents in amphibole and clinopyroxene were calculated by their ideal stoichiometries.

Whole-rock major element compositions were determined by X-ray fluorescence spectrometers (XRF) at the ALS Chemex Guangzhou Co Ltd. in China. The analytical precision was better than 5%. Whole-rock trace elements were analyzed using a Perkin-Elmer Sciex ELAN DRC-e ICP-MS at the SKLODG. The powdered samples (50 mg) were dissolved with HF + HNO_3 mixture in high-pressure Teflon Bombs at ~190 °C for 48 h. Rh was used as an internal standard to monitor signal drift during counting. The analytical precision was generally better than 10%. Whole-rock Sr and Nd isotopic analysis were spiked and dissolved in Teflon bombs with a mixture of HF, HNO_3 and $HClO_4$, and separated by convention cation-exchange techniques. The isotopic measurements were performed on a Nu Plasma multicollector mass spectrometry (MC–ICP–MS) at the State Key Laboratory of Environmental Geochemistry (SKLEG), IGCAS. Mass fractionation correction for Sr and Nd isotopic ratios were based on values of $^{86}Sr/^{88}Sr = 0.1194$ and $^{146}Nd/^{144}Nd = 0.7219$. The Sr standard solution (NBS987) was analyzed five times and yields $^{87}Sr/^{86}Sr$ ratio of 0.710263 ± 0.000014 (2σ). The Nd standard solution (JNDI) was analyzed five times and yields $^{143}Nd/^{144}Nd$ ratio of 0.512084 ± 0.000010 (2σ). The measured results of the USGS standard rock BCR-2 during this study were $^{87}Sr/^{86}Sr = 0.705134 \pm 0.000016$ (2σ) and $^{143}Nd/^{144}Nd = 0.512637 \pm 0.000012$ (2σ), which are within the range of the recommended values (http://georem.mpch-mainz.gwdg.de/sample_query_pref. asp).

5. Analytical results

5.1. Zircon SIMS U—Pb ages and Hf—O isotopes

The U—Pb ages and Hf—O isotopes of zircons from the Gaojiacun and Tongde intrusive complexes are listed in Table S2 and Table S3, respectively. The rock types of the samples from the Gaojiacun and Tongde complexes are gabbrodiorite and diorite/ quartz diorite, respectively.

The cathodoluminescence (CL) images show that the zircon crystals from the Gaojiacun are euhedral to subhedral, with oscillatory or planar zonation (Fig. 2). The grain sizes are from 100 μm to 300 μm in length, with aspect ratios from 1:1 to 5:1. In the CL images, some of these zircon grains have a dark core or a bright rim. These areas were avoided during in-situ analysis. The Gaojiacun zircons contain 22–126 ppm U and 9–121 ppm Th, with Th/U from 0.41 to 0.93. The zircon grains from three samples (GJC1603, GJC1607 and GJC1612) collected at different locations within the Gaojiacun complex yield similar concordant U—Pb ages of 822 ± 6 Ma (2σ; MSWD = 0.4, n = 14), 820.4 ± 6.2 Ma (2σ, MSWD = 0.84, n = 13) and 818.6 ± 5.9 Ma (2σ, MSWD = 0.55, n = 15), respectively (Table 1; Fig. 3a–c). The initial $\varepsilon_{Hf}(t)$ values of these zircons, calculated using the U—Pb ages, are from +4.9 to +7.1, with an average of 6.26 ± 0.52 (Table 1). The $\delta^{18}O$ values of these zircons are from 6.5 to 7.6 ‰, with an average value of 6.96 ± 0.31‰ (Fig. 4), which are significantly higher than the mantle value ($\delta^{18}O = 5.3 \pm 0.6$‰; Valley et al., 2005).

The CL images of zircon crystals separated from quartz diorite (TD1601) and diorite (TD1608) of the Tongde complex are also illustrated in Fig. 2. They are subhedral, with oscillatory and planar zonation. The crystal sizes are from 100 μm to 400 μm in length, with aspect ratios from 1:1 to 4:1. The analyzed zircon grains are free of an inherited core. These zircons contain 60–936 ppm U and 30–1223 ppm Th, with Th/U from 0.26 to 1.93. The zircons from the quartz diorite (TD1601) and diorite (TD1608) yield similar concordant U—Pb ages of 819 ± 5 Ma (2σ, MSWD = 5, n = 15) and 816.2 ± 5.3 Ma (2σ, MSWD = 1.8, n = 15), respectively (Table 1; Fig. 3d–e). The initial $\varepsilon_{Hf}(t)$ values, calculated using the zircon U—Pb ages, are from +3.8 to +5.3, with an average of 4.81 ± 0.39 (Table 1). The $\delta^{18}O$ values of these zircons are from 5.1 to 6.0‰, with an average value of 5.69 ± 0.18‰ (Fig. 4), which is within error of the mantle value ($\delta^{18}O = 5.3 \pm 0.6$‰; Valley et al., 2005).

5.2. Zircon trace elements

Zircon trace element compositions are given as online supplementary data (Table S4). The data show a weak negative correlation between Hf and Ti contents in zircons from each sample. The zircon Ce/Ce* [Ce/(La × Pr)$^{1/2}$] and Eu/Eu* [Eu/(Sm × Gd)$^{1/2}$] ratios of all samples vary from 40 to 1290 and from 0.07 to 0.45, respectively. Between the Gaojiacun and Tongde complexes, zircons from the former have lower total rare earth element abundances than those from the latter, but they are all characterized by significant HREE enrichments and negative Eu anomalies (Fig. S2). Negative Ce anomalies are present in some of the zircons from Gaojiacun but are absent in the zircons from Tongde.

5.3. Mineral chemistry

The chemical compositions of pyroxene, amphibole and plagioclase of gabbrodiorite from Gaojiacun and diorite from Tongde are provided as supplementary data (Table S5). The clinopyroxene crystals of the Gaojiacun samples have compositions similar to augite, with Mg# [100 × Mg/(Mg + Fe^{tot}), molar] varying from 69 to 71 (Fig. S3a). Coexisting orthopyroxene crystals have En [100 × Mg/(Mg + Fe + Ca), molar] varying from 50 to 60. Coexisting plagioclase crystals have anorthite contents [An = 100 × Ca/(Ca + Na), molar] varying from 42.6 to 59.6. Coexisting amphibole grains have compositions varying from

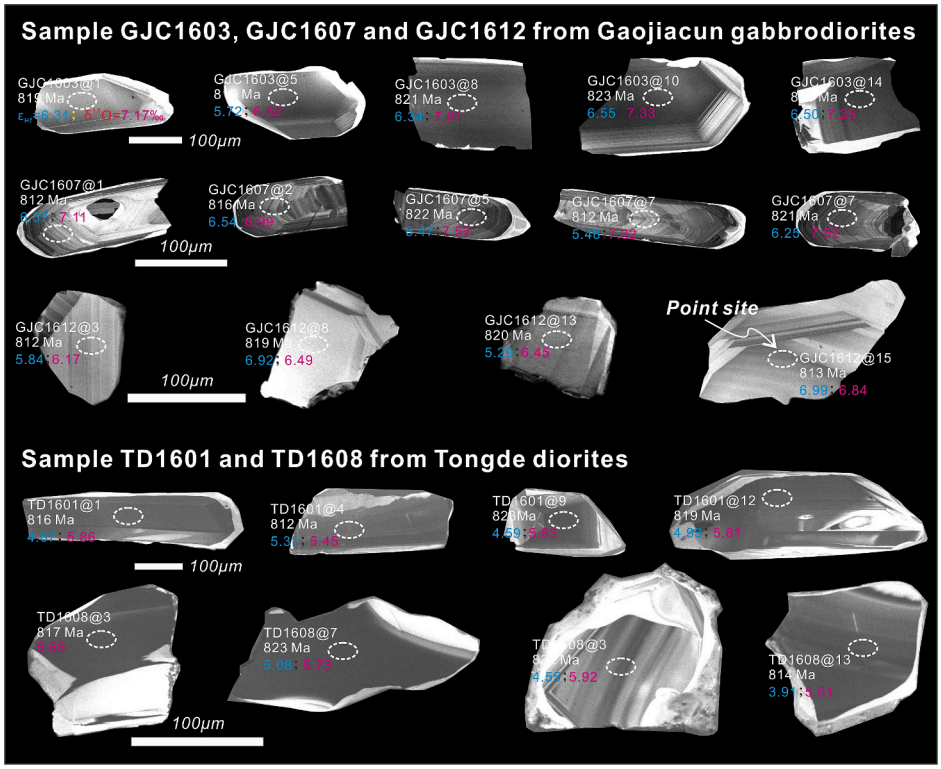

Fig. 2. Cathodoluminescence (CL) images of zircons from Gaojiacun gabbrodiorites and Tongde diorites, with in-situ analytical results: $^{206}Pb/^{238}U$ age in white, ε_{Hf} in blue and $\delta^{18}O$ in magenta. (For interpretation of the references to colour in this figure legend, the reader is referred to the web version of this article.)

Table 1
U—Pb concordia ages and average Hf—O isotopic compositions of zircons from Gaojiacun gabbrodiorites and Tongde diorites.

Sample no.	Rock type	Concordia age (Ma)	2σ (N[a])	$^{176}Hf/^{177}Hf$ (1sd)	$(^{176}Hf/^{177}Hf)_i$ (1sd)	$\varepsilon_{Hf}(t)$ (1sd, N[a])	$\delta^{18}O$ (‰) (1sd, N[a])
GJC1603	Gabbrodiorite	822	6 (14)	0.282459 (0.000011)	0.282439 (0.000008)	6.36 (0.30, 18)	7.04 (0.17, 18)
GJC1607	Gabbrodiorite	820.4	6.2 (13)	0.282439 (0.000017)	0.282427 (0.000016)	5.93 (0.56, 16)	7.23 (0.20, 20)
GJC1612	Gabbrodiorite	818.6	5.9 (15)	0.282450 (0.000014)	0.282441 (0.000015)	6.42 (0.53, 22)	6.64 (0.16, 22)
TD1601	Quartz diorite	819	5.5 (15)	0.282433 (0.000013)	0.282398 (0.000007)	4.91 (0.26, 17)	5.67 (0.21, 18)
TD1608	Diorite	816.2	5.3 (15)	0.282426 (0.000019)	0.282393 (0.000013)	4.72 (0.46, 18)	5.71 (0.15, 23)

[a] N refers to the number of data points that are used to calculate the concordia age and average Hf—O isotopic compositions of sample; The initial $(^{176}Hf/^{177}Hf)_i$ and $\varepsilon_{Hf}(t)$ values are calculated at t = 820 Ma.

hornblende to edenite and pargasite, with Mg# varying from 54 to 63 and ($Na_2O + K_2O$) contents from 1.7 wt% to 2.6 wt% (Fig. S3b). The compositions of clinopyroxene and plagioclase of the Tongde diorite and the Gaojiacun gabbrodiorite are similar. Amphibole crystals from the Tongde diorites have compositions varying from hornblende to pargasite (Fig. S3b).

5.4. Whole-rock chemical and isotopic compositions

The major-trace element and Sr—Nd isotope compositions of the Gaojiacun gabbrodiorite and Tongde diorite are provided as supplementary data (Table S6). The variations of whole-rock major oxide abundances (recalculated to 100% free of loss-on-ignition) are illustrated in Fig. S4. Our new data plus the previously reported data show that the gabbrodiorites in the Gaojiacun outer zone contain 2.7–8.0 wt% MgO, 43.6–54.3 wt% SiO_2, 14.2–20.0 wt% Al_2O_3, 2.7–12.6 wt% CaO and 2.5–5.8 wt% ($Na_2O + K_2O$). As shown in Fig. S4, significant compositional overlaps exist between Gaojiacun gabbrodiorites and Tongde diorites, but the former trend to have higher MgO, $Fe_2O_3^T$ and TiO_2 contents, and lower SiO_2 and ($Na_2O + K_2O$), corresponding to higher abundances of cumulus clinopyroxene and Fe—Ti oxides in the former than in the latter. It is interesting that the diorites of the Tongde batholith have the same major element compositions as the coeval diorite dykes of the Tongde intrusive complex (Fig. S4).

The chondrite-normalized rare earth element (REE) patterns of the Gaojiacun gabbrodiorites and the Tongde diorites are illustrated in Fig. 5a–b. The latter have higher REE abundances and more significant light REE enrichments than the latter. Within the Gaojiacun mafic-ultramafic complex, positive Eu anomaly is present in both types of rocks, but the gabbrodiorite have higher REE contents and more significant light REE enrichments than coexisting ultramafic rocks (Fig. 5a). Similar to the coeval diorite dyke of the Tongde intrusive complex, the diorites of the Tongde batholith are characterized by significant light REE enrichments plus pronounced positive Eu anomaly (Fig. 5b). It is important to note that the Tongde diorites are different from the average REE composition of the Neoproterozoic, so-called adakite-like granitoids in the western rim of the Yangtze block (Zhao et al., 2018) in two aspects: the presence of positive Eu anomaly and a lower degree of fractionation between light and heavy REEs in the former (Fig. 5b).

The mantle-normalized patterns of trace elements for the Gaojiacun gabbrodiorites and the Tongde diorites are illustrated in Fig. 5c–d. Both types of rock are characterized by negative Nb–Ta–Zr–Hf–Ti anomalies, which are the hallmarks of continental arc basalts (CAB) worldwide. The Tongde diorites show positive K–Pb–Sr anomalies, which are typical of classic adakites (Castillo, 2012).

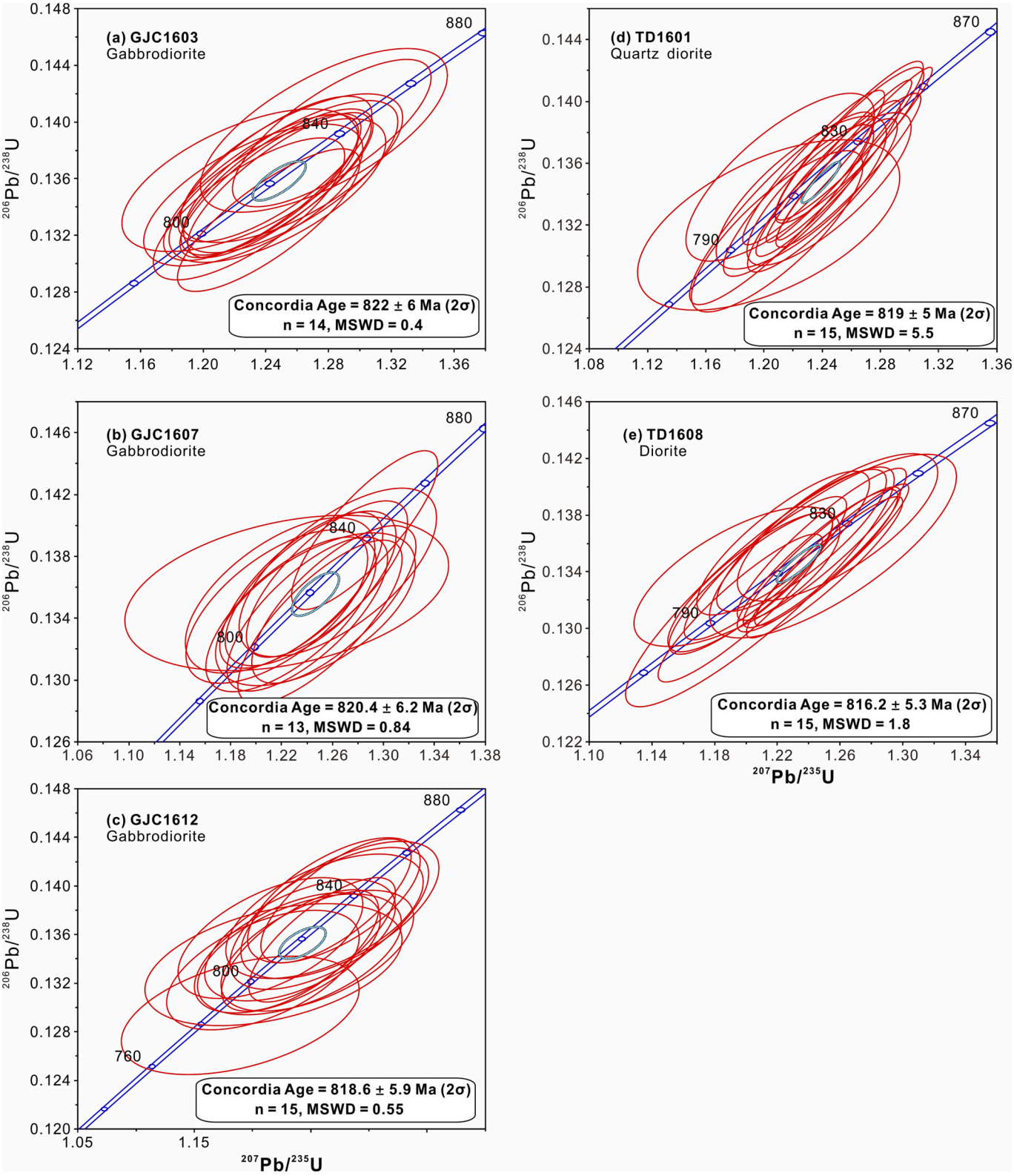

Fig. 3. Zircon U—Pb concordia age diagrams for the Gaojiacun gabbrodiorites (a–c) and Tongde diorites (d–e).

The Gaojiacun gabbrodiorites and the Tongde diorites have similar Sr—Nd isotopic compositions, within or slightly displaced to the right of the field of the mantle array (Fig. 6a). The calculated $\varepsilon_{Nd}(t)$ values (t = 820 Ma) and initial $(^{87}Sr/^{86}Sr)_i$ ratios for the Gaojiacun gabbrodiorites vary from +0.2 to +3.1 and from 0.7046 to 0.7050, respectively. The former overlap the values of coexisting ultramafic rocks whereas the latter are identical to those of the coexisting ultramafic rocks. The Tongde diorites have $\varepsilon_{Nd}(t)$ values from +0.4 to +1.8 and $(^{87}Sr/^{86}Sr)_i$ from 0.7050 to 0.7054. The former are similar to the values of the Tongde diorite dykes whereas the latter tend to be lower than those of the Tongde diorite dykes (Fig. 6a). The $\varepsilon_{Nd}(t)$ values of the Neoproterozoic Gaojiacun and Tongde intrusive complexes are lower than

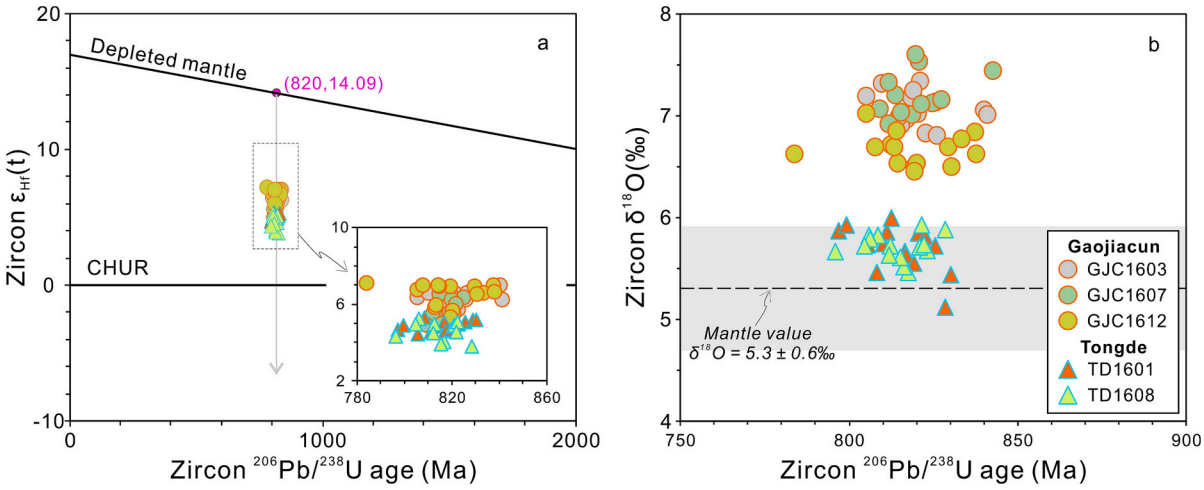

Fig. 4. (a) Zircon ε_{Hf} vs U—Pb age. (b) zircon $\delta^{18}O$ vs U—Pb age. The depleted mantle and chondrite reference lines are from Blichert-Toft and Albarède (1997) and Griffin et al. (2000), respectively. The mantle $\delta^{18}O$ values are from Valley et al. (2005).

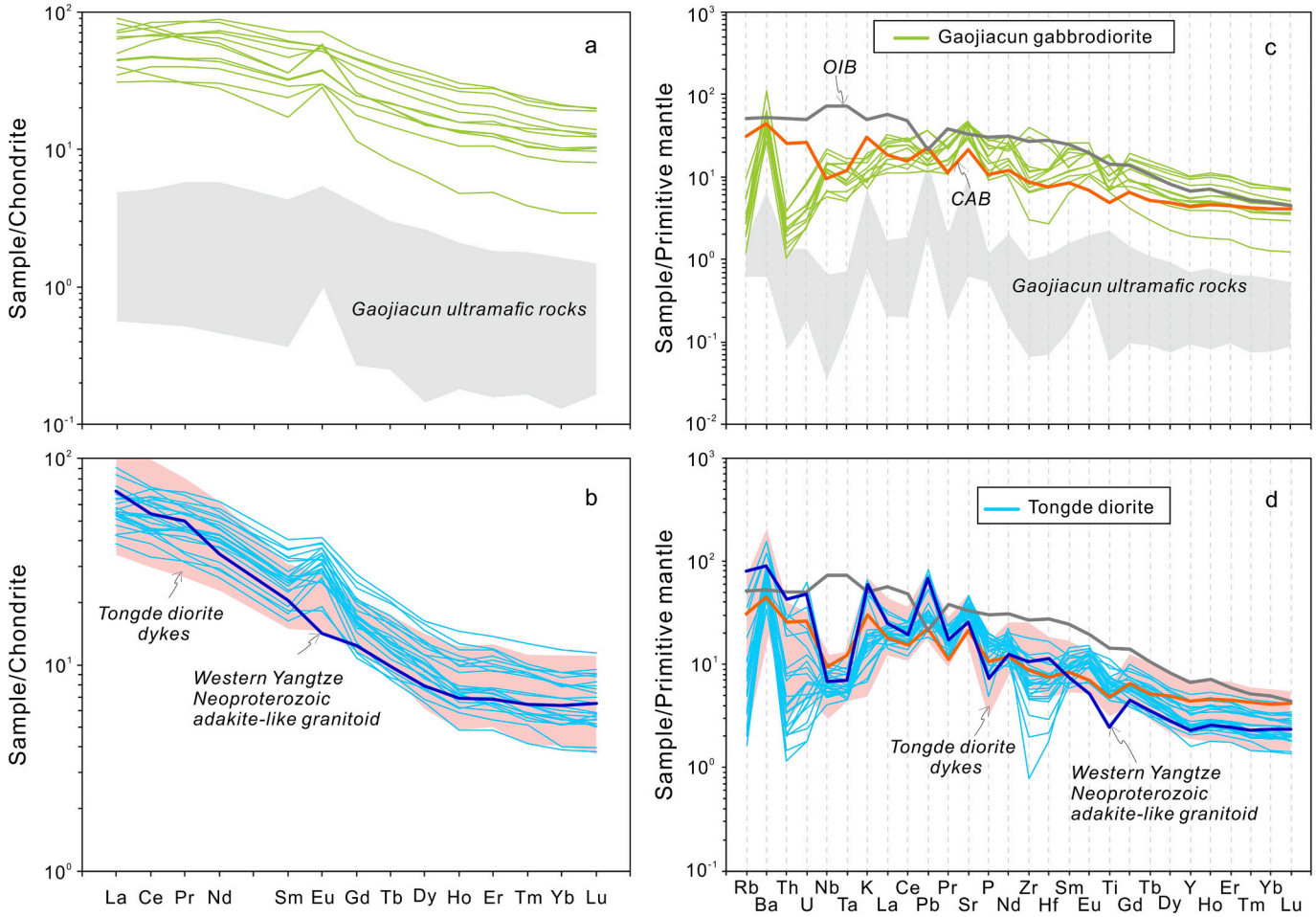

Fig. 5. Chondrite-normalized REE patterns (a–b) and primitive mantle-normalized trace element patterns (c–d) for the Gaojiacun gabbrodiorites and Tongde diorites. Data source: adakite-like granitoids (Zhao et al., 2018), Tongde diorite dykes (Li and Zhao, 2018), Gaojiacun ultramafic rocks (Zhu et al., 2006; Zhou et al., 2006), average oceanic island basalt (OIB) and continental arc basalt (CAB) (https://georoc.mpch-mainz.gwdg.de/georoc; https://search.earthchem.org).

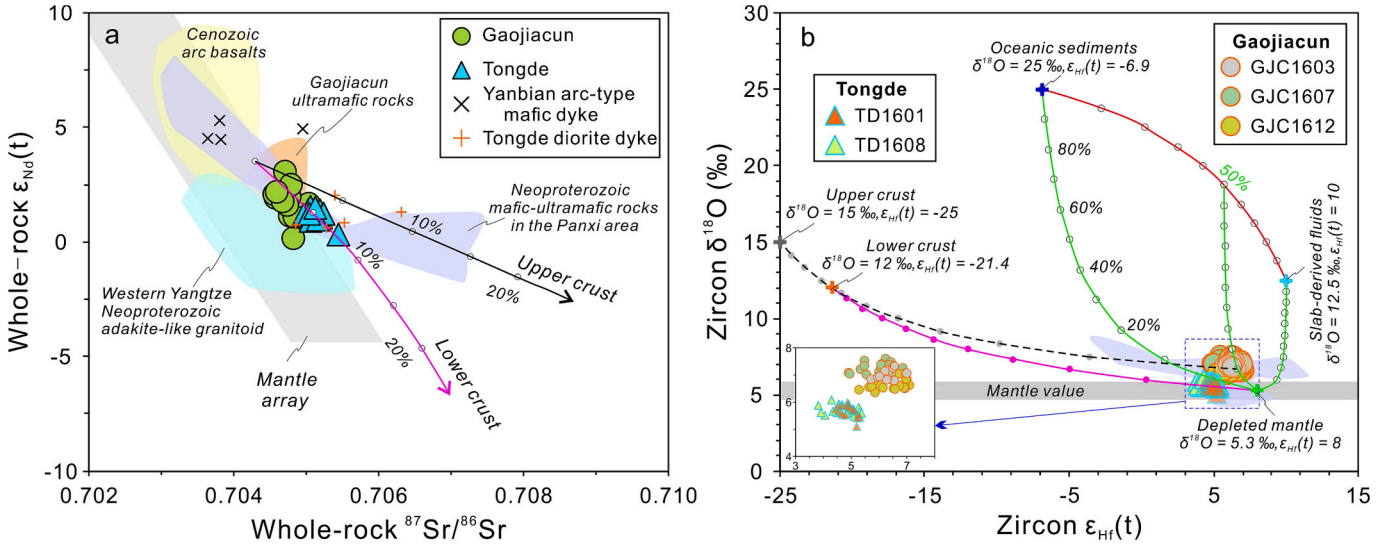

Fig. 6. (a) Whole rock ($^{87}Sr/^{86}Sr)_i$ vs $\varepsilon_{Nd}(t)$, (b) zircon $\varepsilon_{Hf}(t)$ vs $\delta^{18}O$. Data sources: Cenozoic arc basalts (https://georoc.mpch-mainz.gwdg.de/georoc; https://search.earthchem.org), Neoproterozoic mafic-ultramafic rocks in the Panxi area (Zhao et al., 2018), Tongde diorite dykes (Li and Zhao, 2018), Yanbian arc-type mafic dykes (Zhu et al., 2008), Tongde batholith (this study; Munteanu et al., 2010b); Gaojiacun ultramafic rocks (Zhu et al., 2006; Zhou et al., 2006). Parameters used in the mixing calculation: upper crust ($^{87}Sr/^{86}Sr = 0.712$, Sr = 320 ppm; $\varepsilon_{Nd} = -7$, Nd = 27 ppm, $\varepsilon_{Hf}(t) = -25$, Hf = 5.8 ppm, $\delta^{18}O = 15‰$; Plank and Langmuir, 1998; Eiler, 2001; Rudnick and Gao, 2003); lower crust ($^{87}Sr/^{86}Sr = 0.709$, Sr = 348 ppm; $\varepsilon_{Nd} = -26.3$, Nd = 11 ppm, $\varepsilon_{Hf}(t) = -21.4$, Hf = 1.9 ppm, $\delta^{18}O = 12‰$; Dobosi et al., 2003; Rudnick and Gao, 2003; Jiang et al., 2013); depleted mantle ($^{87}Sr/^{86}Sr = 0.7043$, $\varepsilon_{Nd} = -3.5$, $\varepsilon_{Hf}(t) = 8$, Hf = 0.6 ppm, $\delta^{18}O = 5.3‰$); oceanic sediments ($\varepsilon_{Hf} = -6.9$, Hf = 4.1 ppm, $\delta^{18}O = 25‰$; Eiler, 2001; Chauvel et al., 2008; Vervoort et al., 2011); slab-derived fluids ($\varepsilon_{Hf} = 14.5$, Hf = 12 ppm, $\delta^{18}O = 12.5‰$; Eiler, 2001; Kessel et al., 2005; Chauvel et al., 2008; Vervoort et al., 2011). The black and magenta lines correspond to mixing calculation of the depleted mantle with upper crust and lower crust, respectively. The green lines show mixing between the depleted mantle and oceanic sediments and/or slab-derived fluids. The red line refers to mixing between oceanic sediments and slab-derived fluids. The black dashed line represents mixing between upper crust and the depleted mantle enriched by ~10% of a mixing component of oceanic sediments and slab-derived fluids. (For interpretation of the references to colour in this figure legend, the reader is referred to the web version of this article.)

the Neoproterozoic arc-type mafic dykes in the region as well as Cenozoic arc basalts worldwide (Fig. 6a).

6. Discussion

6.1. Arc magmatic tempos

Like elsewhere in the Neoproterozoic circum-Yangtze arc magmatic belt, diorite is much more abundant than the associated mafic-ultramafic rocks at Gaojiacun-Tongde (Fig. 1). New and previously reported zircon U—Pb ages indicate that the Neoproterozoic Gaojiacun mafic-ultramafic complex formed from two episodes of magma emplacement ~19 myr apart from each other. The first episode, which took place at 822 ± 6 Ma, produced a large mafic intrusion with a diameter of ~8 km on surface (Fig. 1c). Based on zircon U—Pb age data from a diorite dyke in the inner zone of the complex (Munteanu et al., 2010a), the second episode took place from ~803 Ma (the age of intercalated diorites) and earlier (the age of the associated ultramafic rocks, which is yet to be determined). These two episodes together produced a mafic-ultramafic complex with a lithological structure like a typical Alaskan-type mafic-ultramafic complex in southern Alaska, such as the Duke Island complex (Irvine, 1967; Thakurta et al., 2008). It is interesting that both the Gaojiacun and Duke Island mafic-ultramafic complexes contain sub-economic Ni—Cu sulfide mineralization in the ultramafic rocks (Zhu et al., 2006; Thakurta et al., 2008).

Our new zircon U—Pb age data show that the Tongde diorite batholith is contemporaneous with the early intrusive phase (the mafic intrusion) of the Gaojiacun complex. These two contemporaneous intrusions form a cross-arc gabbro-diorite suite that can be used to unlock insights into Neoproterozoic arc magmatism at a cratonic margin.

6.2. Magmatic P-T-fO_2 conditions

No correlation between the Al_2O_3 contents and Mg# of amphiboles in the Gaojiacun gabbrodiorites as well as in the Tongde diorites indicates insignificant effect of Tschermak substitution on the amphibole composition, so the Al-in-hornblende barometry of Mutch et al. (2016) can be used to estimate the crystallization pressures for the intrusive rocks. The calculated pressures are 3.0–4.8 kbars for the Gaojiacun gabbrodiorites, and 3.1–4.3 kbars for the Tongde diorites (Table S7).

We have used the Ti-in-zircon equation of Ferry and Watson (2007) to estimate the crystallization temperatures of zircons from the Gaojiacun and Tongde magmas. Since the rocks contain Fe—Ti oxides and/or titanite plus quartz, in the calculation the activities of SiO_2 and TiO_2 are assumed to be 1 and 0.7, respectively. The estimated crystallization temperatures of zircons are from 730 °C to 850 °C, with an average of 791 °C, for the Gaojiacun gabbrodiorites, and from 680 °C to 800 °C, with an average of 749 °C for the Tongde diorites (Table S8; Fig. 7a). We have also used the amphibole-plagioclase geothermometer of Blundy and Holland (1990) to calculate the crystallization temperatures of these minerals for the Gaojiacun gabbrodiorites and the Tongde diorites. The estimated crystallization temperatures of these minerals are from 820 °C to 890 °C for the former and from 780 °C to 800 °C for the latter, which are slightly higher than the estimated crystallization temperatures of coexisting zircons in each intrusion.

We have used the zircon oxybarometer of Loucks et al. (2020), which is based on zircon U, Ti, and Ce compositions, to estimate the oxygen fugacity (fO_2) of the Gaojiacun and Tongde magmatic systems (Table S8). The results are illustrated in Fig. 7a–b. The estimated magmatic redox states for the Tongde diorites are from ΔFMQ+0.3 to ΔFMQ+1.7, with an average of ΔFMQ+1.0, which is within the range of Cenozoic arc basalts (ΔFMQ+1.0 to ΔFMQ+1.6; Brounce et al., 2014). In contrast, the estimated magmatic redox states for the Gaojiacun gabbrodiorites are from ΔFMQ-1.8 to ΔFMQ +0.3, with an average of

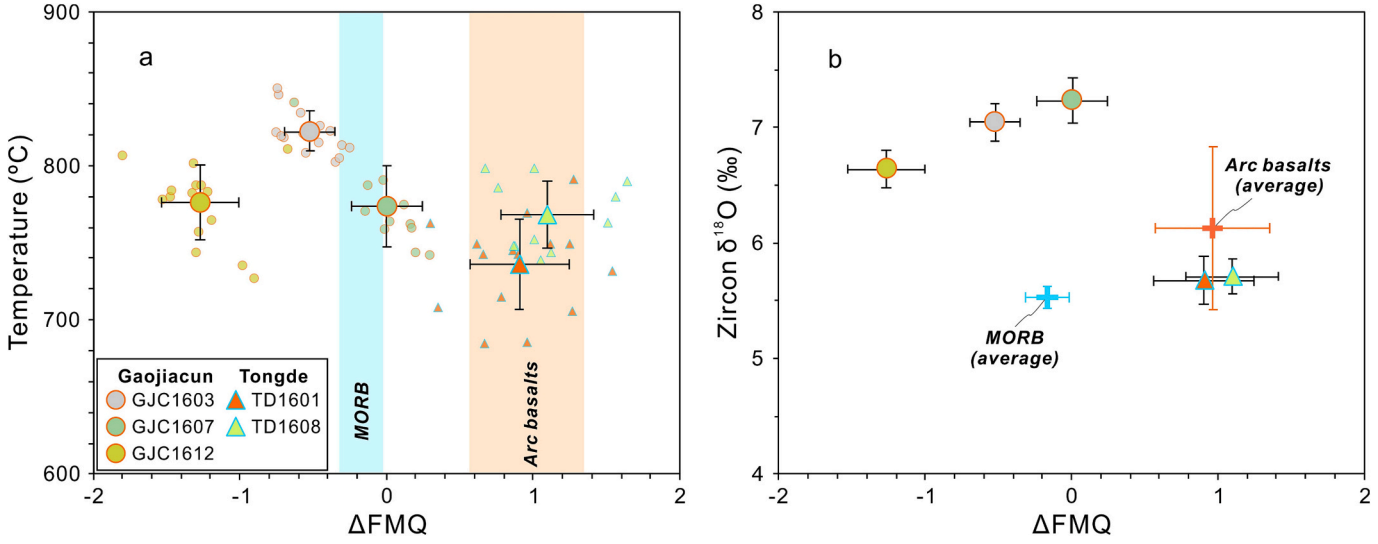

Fig. 7. (a) Estimated magmatic oxygen fugacity vs zircon crystallization temperature. (b) Estimated oxygen fugacity vs zircon $\delta^{18}O$. Data source: ΔFMQ of MORB (mid-ocean ridge basalts) and arc basalts are from Cottrell et al. (2021); Oxygen isotopic data source of MORB and arc basalts are listed in supplementary Text S1. Error bars refer to standard deviation of 1α.

ΔFMQ-0.7, which is significantly lower than those of Cenozoic arc basalts as well as those of mid-ocean ridge basalts (ΔFMQ-0.17; Cottrell et al., 2021).

6.3. The role of fractional crystallization

In theory, fractional crystallization of Fe—Mg silicate minerals such as olivine, clinopyroxene and hornblende without cotectic crystallization of spinel will make the fractionated magma more oxidized, because the early-crystallizing Fe—Mg silicate minerals preferentially remove Fe^{2+} into lattice sites, thereby enriching the liquid in Fe^{3+}. However, crystallization of Fe—Mg silicate minerals from basaltic or andesitic magma is always accompanied by crystallization of Cr-rich or Fe-rich spinel, which preferentially removes Fe^{3+} into lattice sites. The cotectic proportion of Fe—Mg silicate minerals and spinel is a function of the magmatic redox condition. The average cotectic ratio of olivine to spinel in MORBs is estimated to be ~100 (Roeder et al., 2006). We are not aware of any report on the cotectic ratio of Fe—Mg silicate mineral to spinel in arc basalts, but the average ratio should be significantly lower than the MORB value, because arc basalts are overall more oxidized than MORBs (Cottrell et al., 2021).

Several studies of arc volcanic rocks have shown that fractional crystallization does not play a significant role in changing the redox state of arc magma. Kelley and Cottrell (2012) analyzed olivine-hosted melt inclusions from a single eruption of Agrigan volcano, Marianas, and found a positive correlation between $Fe^{3+}/\Sigma Fe$ and MgO in the samples, inconsistent with the result of fractional crystallization. The melt inclusions also show a positive correlation between $Fe^{3+}/\Sigma Fe$ and S concentrations, so these authors attributed the observed variation of magmatic redox states to magma degassing during eruption. Interestingly, geochemical study of Mexican andesites and dacites indicates that fractional crystallization and degassing from the parental magmas cannot explain the observed variation of redox states in the magmas (Crabtree and Lange, 2012). Based on the results from an integrated geochemical investigation of samples from the Central Volcanic Zone of the Andes, which includes melt inclusion $Fe^{3+}/\Sigma Fe$ and whole rock $^{87}Sr/^{86}Sr$, Grocke et al. (2016) conclude that neither fractional crystallization nor crustal contamination played a significant role in controlling the variation of the redox states of these arc magmas.

Based on the fundamental considerations and known natural examples described above, we can rule out that fractional crystallization played a major role in causing the observed large fO_2 variation across the Panxi arc magmatic belt. The effect of degassing on the magmatic redox states of the intrusive rocks from this study are likely negligible and similar, because they were emplaced in the upper crust at similar depths and should have experienced similar degrees of degassing if this process indeed occurred. Therefore, we will not consider the effects of degassing and fractional crystallization any more in the following discussion.

6.4. Isotopic constraints

The Gaojiacun gabbrodiorites and Tongde diorites have major element compositions like typical arc andesites and could have undergone the same processes as andesites. It is well known that andesite may represent a primary arc magma, a differentiated magma, or a hybrid melt produced by mixing between a primary arc basaltic magma and a siliceous melt produced by partial melting of the overriding arc basalts (e.g., Kelemen et al., 2007; Grove et al., 2012; Ducea et al., 2015). Fractional crystallization does not change magma Sr–Nd–Hf–O isotopic compositions, so we need not to evaluate the effect of such process on the isotopic variations in our samples. Since we don't know the compositions of two potential endmembers involved in magma mixing, we cannot evaluate the role of such process in causing the observed magmatic fO_2 variation. Hence, in the following discussion we will focus solely on the effects of crustal contamination and mantle source variation.

The ε_{Nd} values of the Tongde diorite batholith and associated dyke are similar, but the $(^{87}Sr/^{86}Sr)_i$ of these rocks vary significantly (Fig. 6a), which can be explained by the different mobility between Sm—Nd and Rb—Sr during post-magmatic processes. It is well known that Sm and Nd are generally immobile during post-magmatic hydrothermal alteration and weathering, and that Rb and Sr are mobile during these processes. If a rock has lost some Rb during these processes, the calculated $(^{87}Sr/^{86}Sr)_i$ will increase. If a rock has gained some Rb, the opposite result is expected. To avoid such effect, we will focus on the ε_{Nd} data in the following discussion.

As shown in Fig. 6a, the ε_{Nd} values of the Gaojiacun gabbrodiorites and the coeval Tongde diorites overlap significantly, but the former tend to have higher values than the latter overall. The difference can be reproduced by variable degrees of assimilation-fractional crystallization (AFC) process in a MUSH zone at the boundary between the upper mantle and the lower crust, or in the overlying crustal section through which magma ascends. The parental magma for the Tongde diorite

experienced slightly higher degrees of AFC (~5%) than that for the Gaojiacun gabbrodiorite. In the calculation, we use the average composition of the continental lower crust from Jiang et al. (2013) as the contaminant. The modelling result based on the isotopic data is generally consistent with the mineralogical and petrological variations, which indicates that the Tongde diorite formed from magma with more evolved composition relative to the Gaojiacun gabbrodiorite.

It is intriguing that zircons from the Gaojiacun gabbrodiorite have slightly higher ε_{Hf} values and significantly higher $\delta^{18}O$ values than those from the Tongde diorites (Fig. 6b). Apparently, this is inconsistent with variable degrees of crustal contamination, but can be well explained by different subduction inputs to the mantle wedge during magma generation at different locations. As shown in Fig. 6b, the isotope variations are consistent with more subducting oceanic sediment addition to the mantle wedge during magma generation at Gaojiacun than at Tongde. Mixing calculations indicate 10–15% of subduction inputs (mixing components of oceanic sediment with slab-derived fluid) for the Gaojiacun gabbrodiorites and ~ 5% of lower crustal contamination for the Tongde diorites, respectively.

6.5. Subducting organic matter-rich sediments beneath Gaojiacun

As shown in Fig. 7b, the zircon data indicate that the magmatic fO_2 values of the Tongde batholith are similar to the value of typical arc basalts ($\delta^{18}O = 6.13 \pm 0.71‰$; $\Delta FMQ+0.96 \pm 0.39$; Cottrell et al., 2021), whereas the magmatic fO_2 values of the Gaojiacun intrusion are much lower, even lower than the average MORB value ($\Delta FMQ-0.2$; Cottrell et al., 2021). There are two plausible explanations for the unusually low fO_2 of the Gaojiacun magma: (a) contamination of relatively oxidized arc magma with organic matter (OM) rich sedimentary rocks in the upper crust, which was used before to explain a reduction phenomenon of arc magma in Japan (Tomkins et al., 2012), or (b) OM-rich subducting sediments in the mantle source. It is important to note that these two competing models are based on the same fundamental that organic carbon dissolved in magma is predominantly bonded with oxygen, thereby making the magma more reduced (Tomkins et al., 2012). The main difference between these two models is the locations at which the reduction process takes place, one is at the mantle source and the other is at the magma plumbing system in the overriding upper crust. In this study we do not adopt the model of Tomkins et al. (2012) for two reasons: (1) there is no report of OM-rich sedimentary rocks with very high $\delta^{18}O$ in the Panxi region, and (2) the zircon Hf—O isotope data are more consistent with our new model, as justified below.

As shown in Fig. 6b, the unusual combination of $\delta^{18}O$ and ε_{Hf} values of zircons from the Gaojiacun gabbrodiorite can be well reproduced by mixing between mantle-derived melt and subducting oceanic sediments-derived melt during magma generation, followed by minor contamination with the lower crust in the MUSH zone, but is inconsistent with crustal contamination alone. Thus, we tentatively conclude that the relatively reduced condition of the parental magma for the Gaojiacun gabbronorites is mainly due to the involvement of OM-rich subducting oceanic sediments during magma generation. Detailed isotopic study of the pre-magmatic sedimentary rocks in the region are needed to further test our preferred model.

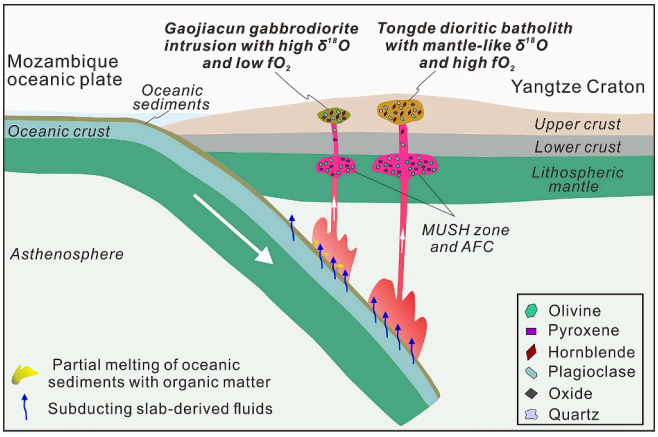

Fig. 8. A conceptual model for the Panxi Neoproterozoic arc magmatic system. The distance between the two complexes is exaggerated. See text for further explanations.

6.6. A model for Neoproterozoic arc magmatism

The zircon U—Pb age data indicate that the Gaojiacun gabbroic intrusion and the Tongde dioritic batholith formed above a Neoproterozoic subduction zone beneath the western margin of the Yangtze craton, with the former occurring closer to the trench than the latter (Fig. 8). As the eastward subduction of Mozambique oceanic slab progressed (Zhao and Zhou, 2007), some subducting oceanic sediments containing abundant organic matter became trapped in the overlying mantle wedge beneath the crust at Gaojiacun. At this location, the release of slab-derived fluids induced partial melting of the overlying mantle wedge as well as the trapped oceanic sediments with abundant organic matter, producing a relatively reduced silicate melt with elevated $\delta^{18}O$ values. Such magma underwent minor AFC in the MUSH zone at the boundary between the upper mantle and the lower crust before ascending to the upper crust to form the Gaojiacun gabbroic intrusion at ~820 Ma. Meanwhile, flux melting of the mantle wedge further to the east produced a silicate melt with $\delta^{18}O$ and fO_2 similar to those of typical arc basalts ($\delta^{18}O = 6.13 \pm 0.71‰$; $\Delta FMQ+0.96 \pm 0.39$). This magma underwent more extensive AFC in the MUSH zone than the Gaojiacun magma, and then ascended to the upper crust to form the Tongde diorite batholith.

7. Conclusions

Important findings from this study are listed below.

(1) Zircon U—Pb ages show that the Gaojiacun gabbrodiorite intrusion and the adjacent Tongde diorite batholith were emplaced almost simultaneously at ~820 Ma above a subduction zone beneath the western margin of the Yangtze craton.
(2) Zircons from the Gaojiacun intrusion have much higher ε_{Hf} (6.26 ± 0.52) and $\delta^{18}O$ (6.96 ± 0.31‰) than those from the Tongde batholith ($\varepsilon_{Hf} = 4.81 \pm 0.39$; $\delta^{18}O = 5.69 \pm 0.18‰$).
(3) The magmatic fO_2 estimated from zircon trace element compositions are $\Delta FMQ+1.0$ for Tongde and $\Delta FMQ-0.7$ for Gaojiacun. The former is within the range of modern arc basalts, but the latter is much lower, more reduced than the average MORB.
(4) In light of the associated Hf—O isotopic variations, we attribute the unusually low magmatic fO_2 of the Gaojiacun magma to the involvement of OM-rich subducting sediments during magma generation instead of crustal contamination.
(5) The results from this study show that a single subduction zone can produce both reduced and oxidized magma over very short spatial scales (<10 km).

Supplementary data to this article can be found online at https://doi.org/10.1016/j.chemgeo.2023.121735.

Declaration of Competing Interest

The authors declare that they have no known competing financial interests or personal relationships that could have appeared to influence the work reported in this paper.

Data availability

Data will be made available on request.

Acknowledgments

This study was finally supported by the National Natural Science Foundation of China (Grants 42172092, 42121003, and 42206051) and Guizhou Provincial 2021 Science and Technology Subsidies (No. GZ2021SIG). We thank Juan Wang for help in EMPA, Kai Lu and Jiao Li for zircon U—Pb dating and O isotope analysis by SIMS, Jing Hu and Yan Huang for whole-rock trace element analysis by ICP–MS, and Fang Xiao and Ting Zhou for whole-rock Sr—Nd isotopic analysis by MC–ICP–MS. We are grateful for thorough reviews from two anonymous reviewers and detailed revision guidance from the editor Dr. Sonja Aulbach.

References

Blichert-Toft, J., Albarède, F., 1997. The Lu-Hf isotope geochemistry of chondrites and the evolution of the mantle-crust system. Earth Planet. Sci. Lett. 148, 243–258.
Blundy, J.D., Holland, T.J., 1990. Calcic amphibole equilibria and a new amphibole-plagioclase geothermometer. Contrib. Mineral. Petrol. 104, 208–224.
Brounce, M., Kelley, K., Cottrell, E., 2014. Variations in $Fe^{3+}/\sum Fe$ of Mariana Arc basalts and mantle wedge fO_2. J. Petrol. 55, 2513–2536.
Castillo, P.R., 2012. Adakite petrogenesis. Lithos 134, 304–316.
Chauvel, C., Lewin, E., Carpentier, M., Arndt, N.T., Marini, J.-C., 2008. Role of recycled oceanic basalt and sediment in generating the Hf–Nd mantle array. Nat. Geosci. 1, 64–67.
Cottrell, E., Birner, S.K., Brounce, M., Davis, F.A., Waters, L.E., Kelley, K.A., 2021. Oxygen fugacity across tectonic settings. In: Moretti, R., Neuville, D.R. (Eds.), Magma Redox Geochemistry. Wiley, pp. 33–61.
Crabtree, S.M., Lange, R.A., 2012. An evaluation of the effect of degassing on the oxidation state of hydrous andesite and dacite magmas: a comparison of pre-and post-eruptive Fe^{2+} concentrations. Contrib. Mineral. Petrol. 163, 209–224.
Dobosi, G., Kempton, P.D., Downes, H., Embey-Isztin, A., Thirlwall, M., Greenwood, P., 2003. Lower crustal granulite xenoliths from the Pannonian Basin, Hungary, part 2: Sr–Nd–Pb–Hf and O isotope evidence for formation of continental lower crust by tectonic emplacement of oceanic crust. Contrib. Mineral. Petrol. 144, 671–683.
Du, L., Guo, J., Nutman, A.P., Wyman, D.A., Geng, Y., Yang, C., Liu, F., Ren, L., Zhou, X., 2014. Implications for Rodinia reconstructions for the initiation of Neoproterozoic subduction at ~860 Ma on the western margin of the Yangtze Block: evidence from the Guandaoshan Pluton. Lithos 67–82.
Ducea, M.N., Saleeby, J.B., Bergantz, G., 2015. The architecture, chemistry, and evolution of continental magmatic arcs. Annu. Rev. Earth Planet. Sci. 43, 299–331.
Eiler, J.M., 2001. Oxygen isotope variations of basaltic lavas and upper mantle rocks. Rev. Mineral. Geochem. 43, 319–364.
Ferry, J., Watson, E., 2007. New thermodynamic models and revised calibrations for the Ti-in-zircon and Zr-in-rutile thermometers. Contrib. Mineral. Petrol. 154, 429–437.
Fisher, C.M., Vervoort, J.D., Hanchar, J.M., 2014. Guidelines for reporting zircon Hf isotopic data by LA-MC-ICPMS and potential pitfalls in the interpretation of these data. Chem. Geol. 363, 125–133.
Gao, S., Yang, J., Zhou, L., Li, M., Hu, Z., Guo, J., Yuan, H., Gong, H., Xiao, G., Wei, J., 2011. Age and growth of the Archean Kongling terrain, South China, with emphasis on 3.3 Ga granitoid gneisses. Am. J. Sci. 311, 153–182.
Gill, J.B., 1981. Orogenic Andesites and Plate Tectonics. Springer, Berlin.
Griffin, W., Pearson, N., Belousova, E., Jackson, S.V., Van Achterbergh, E., O'Reilly, S.Y., Shee, S., 2000. The Hf isotope composition of cratonic mantle: LAM-MC-ICPMS analysis of zircon megacrysts in kimberlites. Geochim. Cosmochim. Acta 64, 133–147.
Grocke, S.B., Cottrell, E., De Silva, S., Kelley, K.A., 2016. The role of crustal and eruptive processes versus source variations in controlling the oxidation state of iron in Central Andean magmas. Earth Planet. Sci. Lett. 440, 92–104.
Grove, T.L., Till, C.B., Krawczynski, M.J., 2012. The role of H_2O in subduction zone magmatism. Annu. Rev. Earth Planet. Sci. 40, 413–439.
Hu, Z., Liu, Y., Gao, S., Liu, W., Zhang, W., Tong, X., Lin, L., Zong, K., Li, M., Chen, H., 2012. Improved in situ Hf isotope ratio analysis of zircon using newly designed X skimmer cone and jet sample cone in combination with the addition of nitrogen by laser ablation multiple collector ICP-MS. J. Anal. Atom. Spectrom. 27, 1391–1399.
Huang, B., Wang, W., Zhao, J.-H., Khattak, N.U., Huang, S.-F., Lu, G.-M., Xue, E.-K., Sun, L., 2023. Coupled Alkaline High-Nb Mafic Rocks and Adakitic Granodiorites: Products of Neoproterozoic Back-Arc Extension at the Western Margin of the Yangtze Block, South China. Geol. Soc. Am. Bull. https://doi.org/10.1130/B36618.1.
Irvine, T., 1967. The Duke Island ultramafic complex, southeastern Alaska. In: Wyllie, P. J. (Ed.), Ultramafic and Related Rocks. John Wiley and Sons, New York, pp. 84–97.
Jiang, N., Guo, J., Chang, G., 2013. Nature and evolution of the lower crust in the eastern North China craton: a review. Earth-Sci. Rev. 122, 1–9.
Kelemen, P.B., Hanghøj, K., Greene, A.R., 2007. One view of the geochemistry of subduction-related magmatic arcs, with an emphasis on primitive andesite and lower crust. Treat. Geochem. 3, 70. https://doi.org/10.1016/B0-08-043751-6/03035-8. Chapter 18.
Kelley, K.A., Cottrell, E., 2012. The influence of magmatic differentiation on the oxidation state of Fe in a basaltic arc magma. Earth Planet. Sci. Lett. 329–330, 109–121.
Kessel, R., Schmidt, M.W., Ulmer, P., Pettke, T., 2005. Trace element signature of subduction-zone fluids, melts and supercritical liquids at 120–180 km depth. Nature 437, 724–727.
Li, Q.-W., Zhao, J.-H., 2018. The Neoproterozoic high-Mg dioritic dikes in South China formed by high pressures fractional crystallization of hydrous basaltic melts. Precambrian Res. 309, 198–211.
Li, X.H., Liu, Y., Li, Q.L., Guo, C.H., Chamberlain, K.R., 2009. Precise determination of Phanerozoic zircon Pb/Pb age by multicollector SIMS without external standardization. Geochem. Geophys. Geosyst. 10.
Li, X.H., Long, W.G., Li, Q.L., Liu, Y., Zheng, Y.F., Yang, Y.H., Chamberlain, K.R., Wan, D. F., Guo, C.H., Wang, X.C., 2010. Penglai zircon megacrysts: a potential new working reference material for microbeam determination of Hf–O isotopes and U–Pb age. Geostand. Geoanal. Res. 34, 117–134.
Li, X.-H., Li, Z.-X., Sinclair, J.A., Li, W.-X., Carter, G., 2006. Revisiting the "Yanbian Terrane": implications for Neoproterozoic tectonic evolution of the western Yangtze Block, South China. Precambrian Res. 151, 14–30.
Li, X.-H., Faure, M., Lin, W., Manatschal, G., 2013. New isotopic constraints on age and magma genesis of an embryonic oceanic crust: the Chenaillet Ophiolite in the Western Alps. Lithos 160, 283–291.
Liu, Y., Gao, S., Hu, Z., Gao, C., Zong, K., Wang, D., 2010. Continental and oceanic crust recycling-induced melt–peridotite interactions in the Trans-North China Orogen: U–Pb dating, Hf isotopes and trace elements in zircons from mantle xenoliths. J. Petrol. 51, 537–571.
Loucks, R.R., Fiorentini, M.L., Henríquez, G.J., 2020. New magmatic oxybarometer using trace elements in zircon. J. Petrol. 61, egaa034.
Ludwig, K., 2011. Isoplot/Ex, Version 4.15: a geochronological toolkit for Microsoft Excel. Geochronol. Center Berkel. 4, 75.
Morel, M., Nebel, O., Nebel-Jacobsen, Y., Miller, J., Vroon, P., 2008. Hafnium isotope characterization of the GJ-1 zircon reference material by solution and laser-ablation MC-ICPMS. Chem. Geol. 255, 231–235.
Munteanu, M., Wilson, A.H., Yao, Y., Chunnett, G., Luo, Y., 2010a. Sequence of magma emplacement and sulfide saturation in the Gaojiacun–Lengshuiqing intrusive complex (SW China). Mineral. Deposita 45, 517–529.
Munteanu, M., Wilson, A., Yao, Y., Harris, C., Chunnett, G., Luo, Y., 2010b. The Tongde dioritic pluton (Sichuan, SW China) and its geotectonic setting: regional implications of a local-scale study. Gondwana Res. 18, 455–465.
Mutch, E., Blundy, J., Tattitch, B., Cooper, F., Brooker, R., 2016. An experimental study of amphibole stability in low-pressure granitic magmas and a revised Al-in-hornblende geobarometer. Contrib. Mineral. Petrol. 171, 1–27.
Niu, J., Li, Z.-X., Zhu, W., 2016. Palaeomagnetism and geochronology of mid-Neoproterozoic Yanbian dykes, South China: implications for a *c.* 820–800 Ma true polar wander event and the reconstruction of Rodinia. Geol. Soc. Lond., Spec. Publ. 424, 191–211.
Plank, T., Langmuir, C.H., 1998. The chemical composition of subducting sediment and its consequences for the crust and mantle. Chem. Geol. 145, 325–394.
Qi, H., Zhao, J.-H., Johnson, T.E., 2023. The Fundamental Role of H_2O in the Generation of Coeval Sodic and Potassic Granitoids at Continental Arcs: An Example from the Yangtze Block, South China. J. Petrol. 64.
Richards, J.P., 2015. Tectonic, magmatic, and metallogenic evolution of the Tethyan orogen: from subduction to collision-ScienceDirect. Ore Geol. Rev. 70, 323–345.
Roeder, P., Gofton, E., Thornber, C., 2006. Cotectic proportions of olivine and spinel in olivine-tholeiitic basalt and evaluation of pre-eruptive processes. J. Perol. 47, 883–900.
Roger, F., Jolivet, M., Malavieille, J., 2010. The tectonic evolution of the Songpan-Garzê (North Tibet) and adjacent areas from Proterozoic to present: a synthesis. J. Asian Earth Sci. 39, 254–269.
Rudnick, R.L., Gao, S., 2003. Composition of the continental crust. In: Rudnick, R.L. (Ed.), The Crust. Treatise on Geochemistry, vol. 3. Elsevier, Amsterdam, pp. 1–64.
Stern, R.J., 2008. Neoproterozoic crustal growth: the solid Earth system during a critical episode of Earth history. Gondwana Res. 14, 33–50.
Sun, W., 2009. The Neoproterozoic Yanbian Group and Associated Plutons in the Western Yangtze Block, SW China (Doctoral Dissertation). The University of Hong Kong, Hong Kong, China.
Thakurta, J., Ripley, E.M., Li, C., 2008. Geochemical constraints on the origin of sulfide mineralization in the Duke Island Complex, southeastern Alaska. Geochem. Geophys. Geosyst. 9.
Tomkins, A.G., Rebryna, K.C., Weinberg, R.F., Schaefer, B.F., 2012. Magmatic sulfide formation by reduction of oxidized Arc Basalt. J. Petrol. 53, 1537–1567.
Valley, J., Lackey, J., Cavosie, A., Clechenko, C., Spicuzza, M., Basei, M., Bindeman, I., Ferreira, V., Sial, A., King, E., 2005. 4.4 billion years of crustal maturation: oxygen isotope ratios of magmatic zircon. Contrib. Mineral. Petrol. 150, 561–580.
Vervoort, J.D., Plank, T., Prytulak, J., 2011. The Hf–Nd isotopic composition of marine sediments. Geochim. Cosmochim. Acta 75, 5903–5926.
Wang, M., Nebel, O., Wang, C.Y., 2016. The flaw in the crustal 'zircon archive': mixed Hf isotope signatures record progressive contamination of late-stage liquid in mafic–ultramafic layered weiweintrusions. J. Petrol. 57, 27–52.
Woodhead, J., Hergt, J., Shelley, M., Eggins, S., Kemp, R., 2004. Zircon Hf-isotope analysis with an excimer laser, depth profiling, ablation of complex geometries, and concomitant age estimation. Chem. Geol. 209, 121–135.
Xu, L.-L., Zhu, J.-J., Huang, M.-L., Pan, L.-C., Hu, R., Bi, X.-W., 2022. Genesis of hydrous-oxidized parental magmas for porphyry Cu (Mo, Au) deposits in a postcollisional setting: examples from the Sanjiang region, SW China. Miner. Deposita 1–36.

Yao, J.-H., 2019. Petrogenesis and cu-Ni Sulfide Mineralization of the Gaojiacun and Lengshuiqing Mafic-Ultramafic Intrusions in the Western Margin of the Yangtze Craton in China (Doctoral Dissertation). Institute of Geochemistry, Chinese Academy of Sciences, Guiyang, China.

Yao, J.-H., Zhu, W.-G., Li, C., Zhong, H., Bai, Z.-J., Ripley, E.M., Li, C., 2018. Petrogenesis and ore genesis of the Lengshuiqing magmatic sulfide deposit in Southwest China: Constraints from chalcophile elements (PGE, Se) and Sr-Nd-Os-S isotopes. Econ. Geol. 113, 675–698.

Yao, J.-H., Zhu, W.-G., Li, C., Zhong, H., Yu, S., Ripley, E.M., Bai, Z.-J., 2019. Olivine O isotope and trace element constraints on source variation of picrites in the Emeishan flood basalt province, SW China. Lithos 338, 87–98.

Zhao, J.H., Zhou, M.F., 2007. Geochemistry of Neoproterozoic mafic intrusions in the Panzhihua district (Sichuan Province, SW China): implications for subduction-related metasomatism in the upper mantle. Precambrian Res. 152, 27–47.

Zhao, J.-H., Zhou, M.-F., Jian-Ping, Z., 2010. Metasomatic mantle source and crustal contamination for the formation of the Neoproterozoic mafic dike swarm in the northern Yangtze Block, South China. Lithos 115, 177–189.

Zhao, J.-H., Li, Q.-W., Liu, H., Wang, W., 2018. Neoproterozoic magmatism in the western and northern margins of the Yangtze Block (South China) controlled by slab subduction and subduction-transform-edge-propagator. Earth-Sci. Rev. 187, 1–18.

Zhao, J.-H., Zhou, M.-F., Wu, Y.-B., Zheng, J.-P., Wang, W., 2019. Coupled evolution of Neoproterozoic arc mafic magmatism and mantle wedge in the western margin of the South China Craton. Contrib. Mineral. Petrol. 174, 1–16.

Zhao, J.-H., Nebel, O., Johnson, T.E., 2021. Formation and evolution of a neoproterozoic continental magmatic Arc. J. Petrol. 62, 1–53.

Zhou, M.F., Kennedy, A.K., Sun, M., Malpas, J., Lesher, C.M., 2002a. Neoproterozoic Arc-Related Mafic Intrusions along the Northern margin of South China: Implications for the Accretion of Rodinia. J. Geol. 110, 611–618.

Zhou, M.F., Yan, D.P., Kennedy, A.K., Li, Y., Ding, J., 2002b. SHRIMP U–Pb zircon geochronological and geochemical evidence for Neoproterozoic arc-magmatism along the western margin of the Yangtze Block, South China. Earth Planet. Sci. Lett. 196, 51–67.

Zhou, M.F., Ma, Y., Yan, D.P., Xia, X., Zhao, J.H., Sun, M., 2006. The Yanbian Terrane (Southern Sichuan Province, SW China): a Neoproterozoic arc assemblage in the western margin of the Yangtze Block. Precambrian Res. 144, 19–38.

Zhu, W., Zhong, H., Li, X., Liu, B., Deng, H., Qin, Y., 2007. ^{40}Ar–^{39}Ar age, geochemistry and Sr–Nd–Pb isotopes of the Neoproterozoic Lengshuiqing Cu–Ni sulfide-bearing mafic–ultramafic complex, SW China. Precambrian Res. 155, 98–124.

Zhu, W.G., Zhong, H., Deng, H.L., Wilson, A.H., Liu, B.G., Li, C.Y., Qin, Y., 2006. SHRIMP Zircon U-Pb Age, Geochemistry, and Nd-Sr Isotopes of the Gaojiacun Mafic-Ultramafic Intrusive complex, Southwest China. Int. Geol. Rev. 48, 650–668.

Zhu, W.G., Zhong, H., Li, X.H., Deng, H.L., He, D.F., Wu, K.W., Bai, Z.J., 2008. SHRIMP zircon U–Pb geochronology, elemental, and Nd isotopic geochemistry of the Neoproterozoic mafic dykes in the Yanbian area, SW China. Precambrian Res. 164, 66–85.

Zhu, W.G., Li, X.H., Zhong, H., Wang, X.C., He, D.F., Bai, Z.J., Liu, F., 2010. The Tongde Picritic Dikes in the Western Yangtze Block: evidence for Ca. 800-Ma Mantle Plume Magmatism in South China during the Breakup of Rodinia. J. Geol. 118, 509–522.